High-resolution imaging of contact potential difference with ultrahigh vacuum noncontact atomic force microscope

Shin'ichi Kitamura and Masashi Iwatsuki

Citation: Appl. Phys. Lett. **72**, 3154 (1998); doi: 10.1063/1.121577
View online: http://dx.doi.org/10.1063/1.121577
View Table of Contents: http://apl.aip.org/resource/1/APPLAB/v72/i24
Published by the American Institute of Physics.

High-resolution imaging of contact potential difference with ultrahigh vacuum noncontact atomic force microscope

Shin'ichi Kitamura[a] and Masashi Iwatsuki
JEOL Ltd., 1-2 Musashino 3-chome, Akishima, Tokyo 196, Japan

(Received 9 January 1998; accepted for publication 15 April 1998)

An ultrahigh vacuum scanning Kelvin probe force microscope (UHV SKPM) utilizing the gradient of electrostatic force, was developed based on an ultrahigh vacuum noncontact atomic force microscope (NC-AFM) capable of atomic level imaging, and used for simultaneous observation of contact potential difference (CPD) and NC-AFM images. CPD images of a Si(111) surface with Au deposited, clearly showed the potential difference in phases between 7×7 and 5×2 structures. When Ag was deposited as a submonolayer on the Si(111) 7×7 reconstructed surface, the atomic level lateral resolution was observed in CPD images as well as in NC-AFM topographic images. © *1998 American Institute of Physics.* [S0003-6951(98)03224-0]

Most of the contact potential difference (CPD) images in the scanning Kelvin probe force microscope (SKPM) using a noncontact atomic force microscope (NC-AFM) are acquired in atmosphere.[1–4] Since CPD originates from the difference in work function on the surfaces of the tip and sample, the work function of the surface of a sample is obtained by measuring the CPD using a tip of which the work function is known. However, the work function varies with surface oxidation and absorption. Thus, in order to accurately monitor the work function of a clean surface as well as the changes in the work function due to deposition, imaging in ultrahigh vacuum (UHV) condition is desired.

In recent years, systems utilizing UHV NC-AFM are powerful enough to verify an atomic resolution.[5–7] High resolution imaging in a typical UHV NC-AFM uses a cantilever whose spring constant is relatively high (> a few N/m). Using such a cantilever, it is more efficient and accurate to measure the force generated between the tip and sample by detecting a force gradient rather than by directly measuring the cantilever deflection.[8] While the conventional SKPM designed to detect the electrostatic force between the tip and sample by the deflection of the cantilever is unable to achieve an atomic resolution, a SKPM using the force gradient in the same fashion as the UHV NC-AFM may be able to achieve a higher resolution, at least in topographic images, by observing CPD images.

When there is a potential difference U between the tip and sample, the electrostatic force between them is expressed as:

$$F=-1/2U^2\partial C/\partial Z, \tag{1}$$

where C is the effective capacitance between the tip and sample, and Z the distance between the tip and sample. The force gradient is given by

$$\partial F/\partial Z=-1/2U^2\partial^2 C/\partial Z^2. \tag{2}$$

The force gradient is also proportional to the square of the potential difference U, and is effective to detect the CPD.

Thus, we used the force gradient method in NC-AFM for simultaneous observation of CPD and topography images, and successfully achieved atomic level lateral resolution both in CPD and topography images for an Ag evaporated surface on a Si(111) 7×7 structure.

Figure 1 shows a block diagram of the system used in our experiment. The dotted line in the figure indicates the portion of the UHV NC-AFM for topographical imaging,[8] and the solid line indicates the portion added for CPD measurement in this experiment.

In the NC-AFM, the force gradient between the tip and the sample is detected as a shift of the resonance frequency of the cantilever. As shown in Fig. 1, the cantilever is kept oscillating at its resonance frequency by applying positive feedback from the optical deflection detection system to the piezo through the preamplifier (PA), phase shifter (PS), wave form converter (WC) and attenuator (Att.). The frequency of the oscillating cantilever is detected by an FM demodulator (FMD) shown in Fig. 1. The phase-locked loop (PLL) was used as the FMD. Feedback is applied to the Z piezo to keep the constant shift of resonance frequency. The shift of the resonance frequency is determined by the reference voltage (Ref. V) of the error amplifier (EA1).

The resonance frequency of the cantilever will also be changed due to the change of the electrostatic force gradient between the tip and sample caused by a voltage $[V_{dc}+V_{ac}\sin(\omega t)]$ applied to the tip from the oscillator

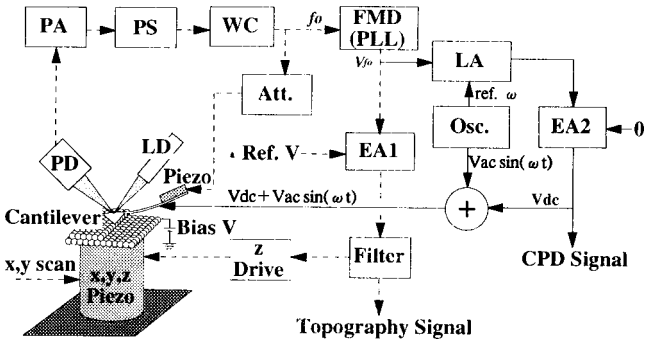

FIG. 1. Block diagram of the NC-AFM system with CPD measurements.

[a]Electronic mail: kitamura@jeol.co.jp

(Osc.) and the error amplifier (EA2). This change will appear as a change of an output of FMD, and a value corresponding to the first derivative of U in formula (2) is detected by the lock-in amplifier (LA). When this output is zero, the effect of the electrostatic force gradient becomes minimum. The dc voltage (V_{dc}) is fed back to the cantilever tip by the EA2 to minimize the electrostatic force gradient. V_{dc} equals CPD between the tip and sample, so the distribution of CPD for the tip is obtained simultaneously with the topography image of NC-AFM.

The NC-AFM system used is a JEOL JAFM-4500XT.[8] A commercial conductive cantilever used is Au sputter-coated with approximately 50 nm of thickness. The cantilever has a resonance frequency of about 250 kHz and a spring constant of about 30 N/m. The vacuum pressure during imaging is less than 10^{-8} Pa. CPD and NC-AFM images are observed simultaneously, and the sample bias voltage at the simultaneous observation is set in advance to a level where V_{dc} becomes roughly zero. The scan speed at the simultaneous observation is 1.7 s/line.

Figures 2(a) and 2(b) show CPD and NC-AFM (topography) images of an Au/Si(111) surface with 7×7 and 5×2 phases in an area of 500×500 nm^2. Figures. 2(c) and 2(d) also show magnified images of CPD and NC-AFM (topography) in an area of 100×100 nm^2. Figures. 2(e) and 2(f) show scanning tunneling microscope (STM) (topography) images in an area of 100×100 nm^2 and 50×50 nm^2, respectively. This surface structure resulted from the evaporation of Au from the cantilever onto the sample surface due to the radiant heat when the sample was flashed in close proximity. In CPD imaging, an ac voltage of 1 kHz frequency with the amplitude of 3 $V_{P\text{-}P}$ was applied to the tip, and no feedback voltage of V_{dc} shown in Fig. 1 was used. As a result, CPD images were observed in a simple way, directly displaying the changes of the output voltage from the lock-in amplifier. The polarity was set so that CPD images would be darkened when the sample bias voltage was negative. Also, for STM imaging, a tunneling current detection line was connected to the tip instead of the voltage line, and 7×7 and 5×2 structures were observed in the empty state. The 7×7 structure in the NC-AFM image of Fig. 2(d) has been observed as a mesh of the 7×7 unit cell. Therefore, the bright and dark regions in CPD images correspond to 7×7 and 5×2 phases, respectively.

The potential difference between 7×7 and 5×2 phases in the CPD image was approximately 0.5 eV, which was calculated by the change of the output voltage from the lock-in amp when the sample bias voltage was changed. The CPD images in Figs. 2(a) and 2(c) demonstrate the potential difference between the different phases. As a result, the 5×2 structure of the Au evaporated sample has a higher work function than the 7×7 reconstruction of Si(111), showing good agreement with the reported data[9] of Au and Si.

Figure 3 shows the changes in the NC-AFM image when different bias voltages were applied to the sample. Sample voltages applied were 2 V (a), 0 V (b), and -1 V (c). As shown in Fig. 3, the contrasts of 7×7 and 5×2 phases were reversed between (a) and (c). It is considered that the electrostatic force gradient on the 7×7 phase at 2 V with the constant height is larger than the 5×2 phase but it is smaller

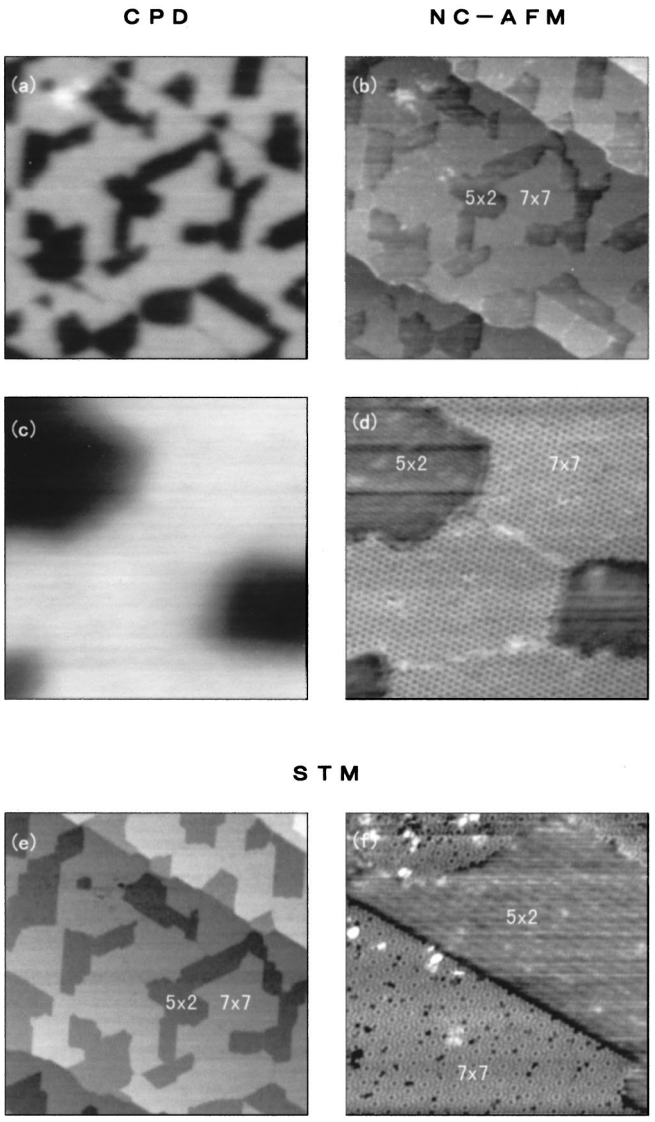

FIG. 2. CPD, NC-AFM, and STM images of the Au/Si (111) surface containing 7×7 and 5×2 phases. The scan sizes were 500×500 nm^2 (a), (b) and 100×100 nm^2 (c), (d) for CPD and NC-AFM images, and 500×500 nm^2 (e) and 50×50 nm^2 (f) for STM images. There was no feedback to the tip dc voltage for CPD measurements. The work function on 5×2 structures was approximately 0.5 eV higher than that on 7×7.

at -1 V. This is probably because each phase has a different CPD for the tip. Therefore, to obtain the NC-AFM image fully to agree with the actual surface topography image, the dc voltage needed to cancel the CPD should be applied between the tip and the sample.

Figures 4 and 5 show the CPD images in (a) and the NC-AFM images in (b) for the Si(111) 7×7 surfaces with Ag evaporation. These images were observed simultaneously in an area of 20×20 nm^2. The Ag coverage in Fig. 4 is larger than that in Fig. 5, and the NC-AFM image demonstrates that most of the area is covered by Ag clusters with an hexagonal island. In this imaging, a voltage feedback was applied to the tip potential to cancel the CPD difference by observing the CPD images to show the direct CPD values for the tip. The voltage modulation for the tip was 2 kHz frequency with the amplitude of 3 $V_{P\text{-}P}$. The contrast in Fig. 4(a) is considered to be the difference in work function between the Ag island and clusters, and the work function of

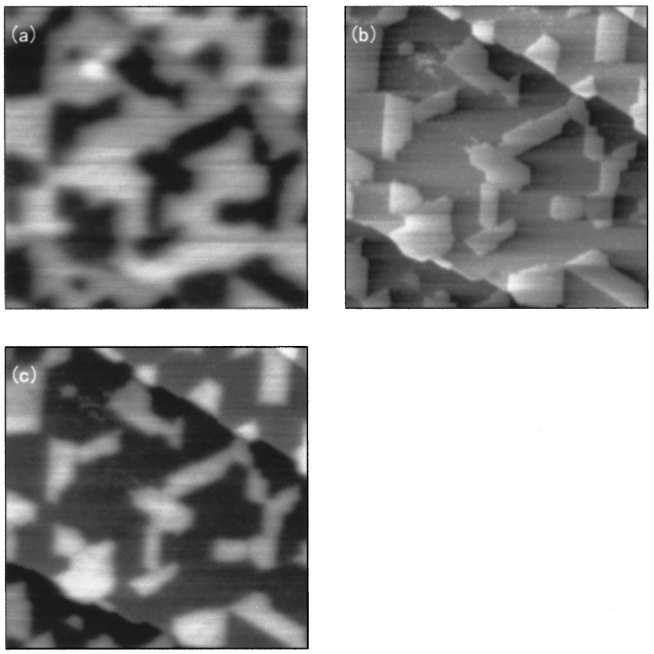

FIG. 3. The change of NC-AFM images when the bias voltage applied to the sample was changed. Voltages applied were (a) 2 V, (b) 0 V, and (c) -1 V.

the island is higher than that of the clusters by approximately 20 meV. The mesh shown at the bottom in Fig. 5 corresponds to a 7×7 unit cell. In the CPD image, most of bright regions correspond to the Ag clusters as marked by the arrows. Thus, the CPD image was observed with an atomic level resolution, discriminating the Ag clusters deposited on the faulted half of 7×7 unit cells. The contrast in Fig. 5 is considered to be the difference in work function between the 7×7 structure and Ag cluster, and the work function of the

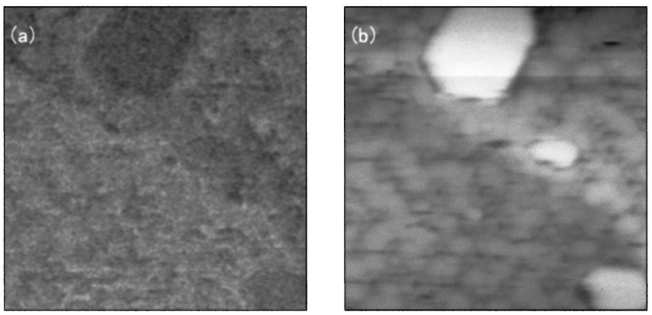

FIG. 4. CPD (a) and NC-AFM (b) images of the Si (111) 7×7 surface with Ag deposits. The scan size was 20×20 nm^2. The work function of the Ag island was approximately 20 meV higher than that of Ag clusters.

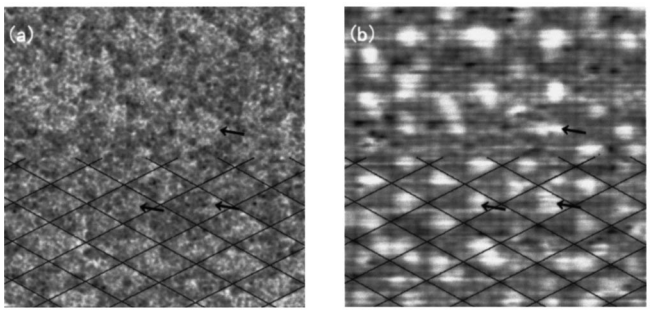

FIG. 5. CPD (a) and NC-AFM (b) images of the Si (111) 7×7 surface with Ag deposits. The Ag coverage was less than Fig. 4. The scan size was 20×20 nm^2. The work function of 7×7 was approximately 10 meV higher than that of the Ag cluster.

7×7 structure is higher than that of the cluster by approximately 10 meV. The results indicate $\phi_{\text{island}}>\phi_{7\times7}>\phi_{\text{cluster}}$, and the values of the work functions show good agreement with the previous data on the work functions,[9] when the Ag cluster is regarded as an Ag polycrystal and the Ag island as an Ag(111) surface.

The CPD images with a potential resolution of less than 10 meV were observed in the SKPM based on the force gradient using the UHV NC-AFM, demonstrating an atomic level resolution. The potential resolution is expected to be improved by increasing the bandwidth of the FM demodulator using a cantilever with a higher resonance frequency and consequently increasing the frequency of the modulation voltage applied to the tip and sample. The absolute value of the work function needs to be measured since the condition of the tip often changes due to distortion and absorption. In the future, however, the use of a metal tip will assure that stable imaging and elemental analysis based on the work functions will be extremely powerful for surface analysis.

[1] J. M. R. Weaver and D. W. Abraham, J. Vac. Sci. Technol. B **9**, 1559 (1991).
[2] M. Nonnenmacher, M. P. O'Boyle, and H. K. Wickramasinghe, Appl. Phys. Lett. **58**, 2921 (1991).
[3] A. K. Henning, T. Hochwitz, J. Slinkman, J. Never, S. Hoffmann, P. Kaszuba, and C. Daghlian, J. Appl. Phys. **77**, 1888 (1995).
[4] T. Hochwitz, A. K. Henning, C. Levey, C. Daghlian, J. Slinkman, J. Never, P. Kaszuba, R. Gluck, R. Wells, J. Pekarik, and R. Finch, J. Vac. Sci. Technol. B **14**, 440 (1996).
[5] F. J. Giessibl, Science **267**, 68 (1995).
[6] S. Kitamura and M. Iwatsuki, Jpn. J. Appl. Phys., Part 2 **34**, L145 (1995).
[7] H. Ueyama, M. Ohta, Y. Sugawara, and S. Morita, Jpn. J. Appl. Phys., Part 2 **34**, L1086 (1995).
[8] S. Kitamura and M. Iwatsuki, JEOL News **32E**, 42 (1995).
[9] *CRC Handbook of Chemistry and Physics*, 65th. ed. (CRC, Boca Raton, FL, 1984), p. E-76.